DEVELOPMENT AND EVALUATION OF A PASSIVE MULTI-LOOP WEARABLE HAND DEVICE FOR NATURAL MOTION

Nina Robson
Mechanical Engineering Department
California State University
Fullerton, California 92834
Email: nrobson@exchange.fullerton.edu

Bin Yun Chen
Mechanical Engineering Department
California State University
Fullerton, California 92834
Email: binyunchen@csu.fullerton.edu

Jong-Seob Won
Department of Mechanical and Automotive Engineering
Jeonju University, South Korea
Visiting Professor, Mechanical Engineering Department
California State University
Fullerton, California 92834
Email: jswon@jj.ac.kr

Gim Song Soh *
Engineering Product Development
Singapore University of Technology
Singapore
Email: sohgimsong@sutd.edu.sg

ABSTRACT

This paper describes the development and evaluation of our passively actuated Closed Loop Articulated Wearable (CLAW) that uses a common slider to passively drive its exo-fingers for use in physical training of people with limited hand mobility. Our design approach utilizes physiological tasks for dimensional synthesis and yields a variety of design candidates that fulfill the desired fingertip precision grasping trajectory. Once it is ensured that the synthesized fingertip motion is close to the physiological fingertip grasping trajectories, performance assessment criteria related to user-device interference and natural joint angle movement are taken into account. After the most preferred design for each finger is chosen, minor modifications are made related to substituting the backbone chain with the wearer's limb to provide the skeletal structure for the customized passive device. Subsequently, we evaluate it for natural joint motion based on a novel design candidate assessment method. A hand prototype is printed, and its preliminary performance regarding natural joint motion, wearability, and scalability are assessed. The pilot experimental test on a range of healthy subjects with different hand/finger sizes shows that the CLAW hand is easy to operate and guides the user's fingers without causing any discomfort. It also ensures both precision and power grasping in a natural manner. This work establishes the importance of incorporating novel design candidate

*Corresponding author.

assessment techniques, based on human finger kinematic models, on a conceptual design level that can assist in finding design candidates for natural joint motion coordination.

1 INTRODUCTION

Over the past several decades, wearable exoskeletons have become a common part of our daily lives [1–5]. The most important design requirement for wearable exoskeleton devices is safety and is usually achieved through some form of mechanical range stopper or through the design itself [6]. The key approach is to design the wearable device with its rotation axis to coincide with the human joint to mimic its workspace. This way, even though there is a failure on the device controller, the exoskeleton will not force the user to move in an unnatural manner resulting in injury to their limbs. There are a few ways in which one could achieve this. The most common manner is to match the joint centers directly [7]. However, this approach requires structural space on the side of the limbs. Alternatively, a remote center of rotation can be considered [8,9]. Alignment and adjustment for human limb size is a significant challenge for the design of these devices as well [10].

Besides safety, the overall weight of the wearable device also plays an important role in the design. Hence, there has been a desire to minimize the number of actuators to reduce the device size and mass, improve its reliability, and lower its cost with simplified mechanical components. This has been accomplished by coupling the motion of multiple joints, with many designs having fewer actuators than degrees of freedom. Such devices termed "underactuated" have shown significant benefits in grasping applications due to the passive adaptability between the degrees of freedom. Under certain conditions, the unconstrained freedoms allow these devices to conform to the environment shape without any need for sensing. Two general types of under-actuated wearable exoskeletons have been proposed in previous works. The first group is based on tendon-driven systems [11, 12], while the second group is based on mechanical linkages [13]. Tendon-driven exoskeletons can usually be designed with compact size and dexterous operation. However, these systems lead to friction and elasticity issues during operation [14–16] and are generally limited to small grasping forces. Linkage mechanisms, on the other hand, are preferable for applications in which high stability and large grasping forces are required [17–19].

It is important to note that while most of the exoskeleton devices in the literature show satisfactory performance, there still does not exist a methodology for the design and assessment of linkage-based systems that incorporate initial anatomical structure, finger-tip trajectory tracking, and joint coordination for human-like motion. The generalization of existing exo-hands to both precision and power grasping and their scalability to different human hand sizes is still challenging. The aforementioned highlights the need to develop design and assessment techniques for under-actuated and passive linkage skeletal structures sized according to the wearer's limb dimensions and closely simulate the human motions. Unlike other wearable device design techniques that use parallel mechanical linkages [20–22], Robson and Soh [23–27] offered a novel alternative approach: a geometric design process to create wearable six- and eight-bar sliders that incorporate initial anthropometric backbone chain and physiological task for natural motion using a minimal number of actuators. This includes all aspects of the geometric design process, from physiological task acquisition, anthropometric backbone chain specification, dimensional synthesis, and user-design candidate interference evaluation. We extend this work by applying recently developed human fingers joint coordination geometric based models, developed by Won and Robson [28] in the assessment of the design candidates to explore the development of robust hand exoskeletons. Finally, we test the extent of the designed exo-hand for generalization to different grasping tasks and its scalability to different human hand/finger sizes.

This paper is organized as follows: Section 2 describes our design methodology for custom wearable assistive devices. Section 3 gives an overview of our assessment approach for natural joint motion. Section 4 presents the design and assessment of our CLAW hand for natural movement. Section 5 illustrates the wearability and scalability test we did with the CLAW hand and discusses the results of the experiments performed. Lastly, we conclude our findings in Section 6.

2 DEVELOPMENT OF CUSTOM WEARABLE ASSISTIVE DEVICES

This section provides an overview of our systematic process for the development of robust, customized assistive devices based on anthropometric limb data and physiological tasks (see Fig. 1).

Our design approach of custom wearable assistive devices is based on anthropometric measurements of the user's limb and is explicitly built to mimic their natural physiological task performance. This information can be easily collected using various motion capture technologies available commercially today. Following this depending on the complexity of the proposed task, a linkage topology (four, six, eight, etc.) is selected. This selection is necessarily dependent on the designer's assessment of the linkage topology suitability to meet the physiological task motion and the safety requirements. Once the dimensional synthesis process is carried out, a set of design candidates is evaluated to identify the most suitable designs. Finally, the most preferred design is modified by replacing the anthropometric backbone chain with the biological limb. A 3D printed prototype can then be manufactured. In what follows, we offer a brief overview of our recent results related to the proposed synthesis procedure, followed by a detailed explanation of the incorporation of candidate assessment for natural joint motion coordination.

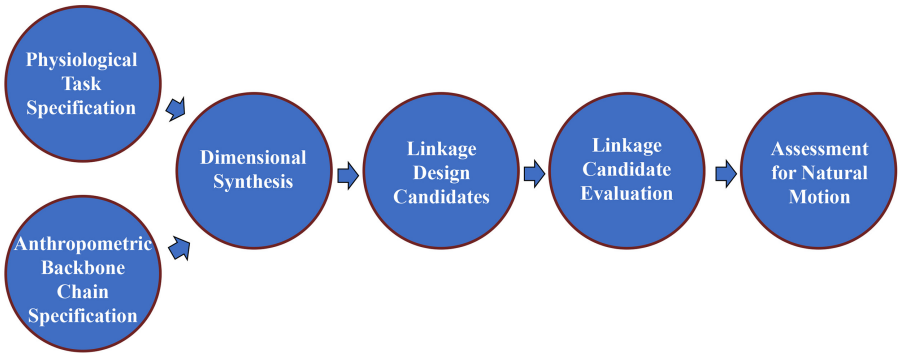

Fig. 1. Our systematic design approach for the development of 3D printed customized wearable assistive devices.

2.1 Human Hand Kinematics

Human hands are highly dexterous and are capable of grasping a wide variety of objects of different shapes and textures. As shown in Fig. 2 on the left, the hand consists of 5 articulated serial chains that comprised of 20 links (inclusive of the ground) and 19 joints with 24 degrees of freedom (DoF). As viewed from the distal end for each finger except for the thumb, the kinematic chain comprises of a 1DoF joint at the distal interphalangeal (DIP), 1DoF joint at the proximal interphalangeal (PIP), and a 2DoF joint at the metacarpophalangeal (MCP) forming a TRR serial chain with its base at the respective MCP joint. If we neglect each finger's abduction/adduction movement at the MCP joints, the kinematic model simplifies to that of a planar 3R chain. The thumb also has a similar kinematic structure from the distal end, which comprises a 1DoF joint at the interphalangeal (IP), 1DoF joint at the metacarpophalangeal (MCP), and a 2DoF joint at the carpometacarpal (CMC).

Similarly, if the abduction/adduction movement at the CMC joint is neglected, the thumb can also be simplified as a planar 3R chain. This interesting kinematic structure can be used to design exoskeleton devices that parallel the limb. Together with the advent of additive manufacturing, this biological structure provides opportunities for the design of a new breed of bioinspired wearable underactuated devices for a variety of purposes, such as assistive, rehabilitative, or augmentative grasping.

2.2 Physiological Task Specification

To be able to go through the desired grasping task, recorded by a motion capture system, two critical poses along the measured markers trajectory, where the local motion is very important for the finger performance, are selected. Typically, for exact synthesis, a velocity at the first pose was defined to represent the fingertip motion direction as tangent as possible to the acquired task trajectory. Acceleration at the second pose is defined at the point of contact between the fingertip and the object as shown in Fig. 2 on the right, where grasping occurs. This builds upon the results of Robson and McCarthy

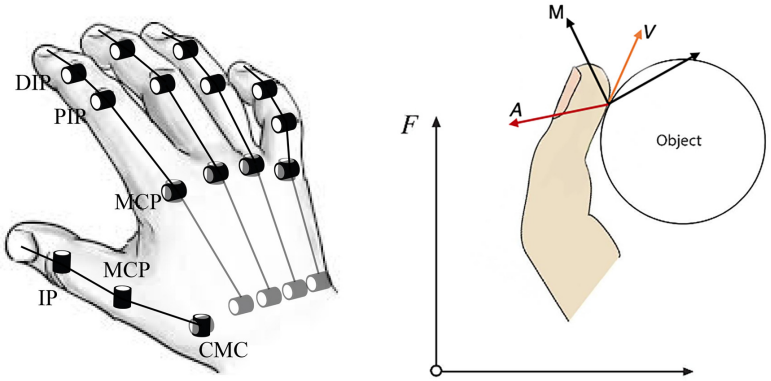

Fig. 2. The kinematics of hand and its associated joints (left). The velocity and acceleration of a task pose are related to the finger-body contact and curvature specifications (right).

(2007) [29], who showed that higher-order derivatives, such as velocities and accelerations, defined in the synthesis task location M relate to the finger-object contact and curvature specifications.

Thus, the physiological task consists of two poses P, two velocities V and one acceleration A specifications, compatible

with the finger tip-object local contact and curvature constraints. These task specifications are parametrized in terms of the frame orientation θ, angular velocity $\dot{\theta}$, angular acceleration $\ddot{\theta}$, as well as the frame origin d_x and d_y, velocity $\dot{d}_x$ and $\dot{d}_y$, and acceleration $\ddot{d}_x$ and $\ddot{d}_y$.

2.3 Dimensional Synthesis of Eight-bar Sliders

The motion generation of eight bar slider mechanisms seeks to constrain a parallel 3R-PRR chain, in which the 3R chain laterally parallels the finger as shown in Fig. 3. This can be achieved by attaching two RR chains to yield an eight-bar

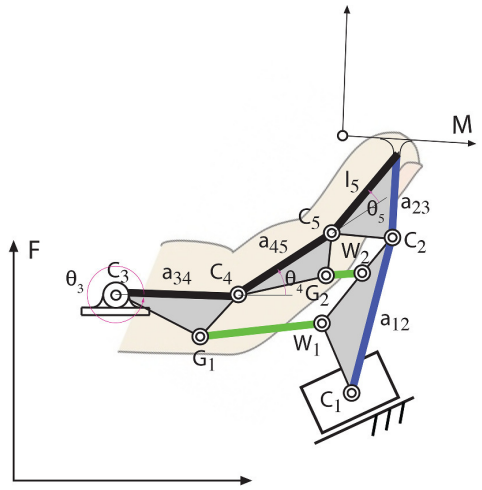

Fig. 3. The linkage-based finger device.

slider linkage [30, 31]. The process consists of 3 steps. First, the various link dimensions for the parallel $\mathbf{C}_1 - \mathbf{C}_5$ chain are specified, such that the resulting parallel linkage moves through the specified physiological task. Note that the dimensions a_{34}, a_{45} and l_5 are based on the human limb anthropometric dimensions. Next, we solve for the robot joint parameters at each specified pose to determine the various links positions, velocity, and acceleration. These matrices then form the task for the motion generation of two RR chains $\mathbf{G}_1\mathbf{W}_1$ and $\mathbf{G}_2\mathbf{W}_2$ to yield an eight-bar slider based exoskeleton.

2.4 User-Design Candidate Interference Evaluation

Based on the above approach, the motion generation of eight-bar sliders can yield a variety of design candidates that fulfill the fingertip precision grasping task trajectory requirements. To ensure wearability, it is important to choose linkage structures that would interface well with the human hand and not impede the intended task. To achieve this, regions $1-3$ are further identified around the finger to sort the two synthesized RR links ($\mathbf{G}_1\mathbf{W}_1$ and $\mathbf{G}_2\mathbf{W}_2$) according to their undesirable or desirable traits as shown in Fig. 4. Region 1 denotes area beside or underneath the finger which are undesirable locations

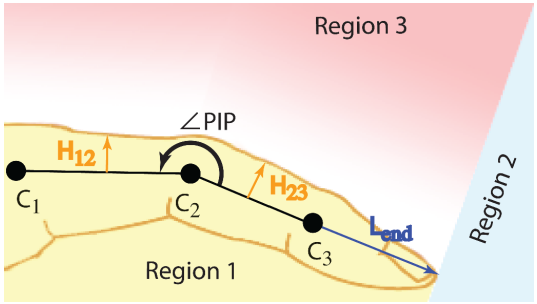

Fig. 4. The desirable and undesirable link pivot regions for a hand exo-limb.

for the fixed and moving pivots $\mathbf{G}_i\mathbf{W}_i$. Having pivots beside the finger, causes a wider linkage envelope and increases the chance of collision between adjacent fingers. Similarly, if the pivots are located underneath the finger, they are likely to collide with the finger itself or the object during flexion. Region 2 denotes designs that have the pivots extending beyond

the tip of the finger. This is undesirable as the linkage would most likely contact with the object first instead of the finger tip during the grasping of larger objects. After eliminating designs with pivots in regions 1 and 2, we rank the remaining linkage candidates, with pivots located in region 3, according to their proximity to the finger. This can be formulated as the sum of the perpendicular distance of $\mathbf{G}_i$ and $\mathbf{W}_i$ to the nearest limb segment $\mathbf{C}_1\mathbf{C}_2$ or $\mathbf{C}_2\mathbf{C}_3$. To determine the perpendicular distance d_i of any pivot $\mathbf{P}_i$, we use the following condition

$$d_i = \begin{cases} \frac{|\mathbf{P}_i\mathbf{C}_2 \times \mathbf{C}_3\mathbf{C}_2|}{|\mathbf{C}_3\mathbf{C}_2|} & \text{if } 0 \leq \angle \mathbf{P}_i\mathbf{C}_2\mathbf{C}_3 \leq \frac{1}{2}\angle PIP \\ \frac{|\mathbf{P}_i\mathbf{C}_1 \times \mathbf{C}_2\mathbf{C}_1|}{|\mathbf{C}_2\mathbf{C}_1|} & \text{if } \frac{1}{2}\angle PIP \leq \angle \mathbf{P}_i\mathbf{C}_2\mathbf{C}_3 \leq \angle PIP \end{cases}$$

The limitation of the described design procedure above is that the resulting solutions do not incorporate/guarantee natural joint coordination of the backbone chain. This is a very important issue since, as previously mentioned, the backbone chain is substituted with the wearer's biological limb at the end of the design procedure to provide the skeletal structure for the custom passive wearable device. Thus, having the anthropometric backbone chain joint motion coordination as close as possible to the human's motion is greatly important. In what follows, we study the coordination of the finger's joint angles to assess the design candidate's capabilities in performing different tasks naturally.

3 DESIGN CANDIDATE ASSESSMENT FOR NATURAL JOINT MOTION

To explore the humans' finger joint coordination, we use our recently developed and validated geometry-based finger kinematic naturalistic model [28] to assess the joint configuration for natural joint motion.

3.1 Joint Configuration Model for the Fingers

In general, it seems that it is natural to grasp a symmetric cylinder-shaped object (a beverage can, for example) with fingers surrounding the outer surface. With this in mind, formulas used to calculate joint angles of a finger during grasping with one control parameter are derived. Depending on the radius of a symmetric object, the joint angles of a finger can be determined. In this work, the distance between the MCP joint and the origin of an object is chosen as a control parameter (in particular R as shown in Fig. 5 since the finger thickness t is a constant). The advantage of this approach is its simplicity in controlling the finger's shape with one parameter. The proposed fingers and thumb kinematic model is based on a hand shape in an open configuration, with each of the fingers in some degrees of flexion. This can be seen as a "naturalistic" shape observed in the human hand. From a modeling viewpoint, it is assumed that the shape of the hand under consideration can be observed when a hand is lightly grasping/encompassing a virtual cylindrical object with each finger in some degree of flexion.

Based on the assumptions made above and the geometry of index finger, the joint rotation angles can be obtained by using trigonometric formulas characterizing plane triangles in Fig. 5. By applying al-Kashi's law of cosines, one gets the following relations:

$$\begin{aligned} a^2 &= b^2 + c^2 - 2bc\cos\alpha \\ b^2 &= c^2 + a^2 - 2ca\cos\beta \\ c^2 &= a^2 + b^2 - 2ab\cos\gamma \end{aligned}$$

where a denotes the distance from O_c to the $i-1$ joint, b the distance from O_c to the i joint and c the distance between the i and $i-1$ joint.

To determine the "naturalistic" joint configuration, we first consider the triangle $O_C J_{1I} J_{2I}$. The angles β_1 and γ_1 are obtained as follows:

$$\begin{aligned} (R+t_{1I})^2 &= (R+t_{0I})^2 + L_1^2 - 2(R+t_{0I})L_1\cos\beta_1 \\ (R+t_{0I})^2 &= (R+t_{1I})^2 + L_1^2 - 2(R+t_{1I})L_1\cos\gamma_1 \end{aligned}$$

Solving equations above for β_1 and γ_1, respectively, gives

$$\beta_1 = \arccos\left(\frac{(R+t_{0I})^2 + L_1^2 - (R+t_{1I})^2}{2(R+t_{0I})L_1}\right) \quad (1)$$

$$\gamma_1 = \arccos\left(\frac{(R+t_{1I})^2 + L_1^2 - (R+t_{0I})^2}{2(R+t_{1I})L_1}\right) \quad (2)$$

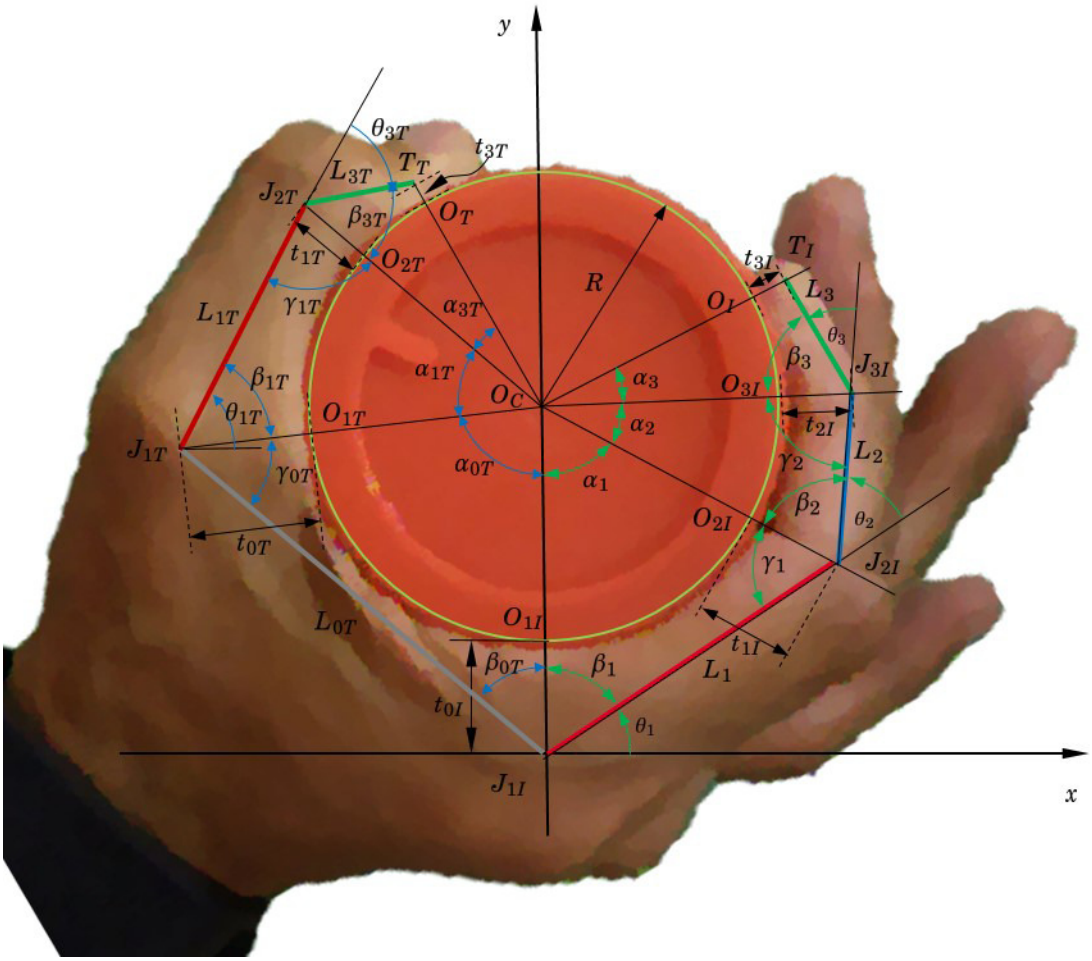

Fig. 5. Schematic of index finger and thumb joint configurations (planar motion is assumed). Note: R, radius of a virtual cylinder object; J_{iI}, $i = 1,2,3$, MCP, PIP and DIP joints, respectively; L_i, length of phalanges of each finger; θ_i, joint rotation angle at each joint; t_{iI}, width from surface to skeleton (joint).

The rotation angle at the MCP joint can be calculated by using Eqn. (1) as follows:

$$\begin{aligned}\theta_1 &= \frac{\pi}{2} - \beta_1 \\ &= \frac{\pi}{2} - \arccos\left(\frac{(R+t_{0I})^2 + L_1^2 - (R+t_{1I})^2}{2(R+t_{0I})L_1}\right) \\ &= f_1(L1, t_{0I}, t_{1I}; R)\end{aligned} \tag{3}$$

Next, consider the triangle $O_C J_{2I} J_{3I}$. The angles β_2 and γ_2 are obtained as follows:

$$\begin{aligned}(R+t_{2I})^2 &= (R+t_{1I})^2 + L_2^2 - 2(R+t_{1I})L_2\cos\beta_2 \\ (R+t_{1I})^2 &= (R+t_{2I})^2 + L_2^2 - 2(R+t_{2I})L_2\cos\gamma_2\end{aligned}$$

Solving equations above for β_2 and γ_2, respectively gives

$$\beta_2 = \arccos\left(\frac{(R+t_{1I})^2 + L_2^2 - (R+t_{2I})^2}{2(R+t_{1I})L_2}\right) \tag{4}$$

$$\gamma_2 = \arccos\left(\frac{(R+t_{2I})^2 + L_2^2 - (R+t_{1I})^2}{2(R+t_{2I})L_2}\right) \tag{5}$$

By using Eqns. (2) and (4), the rotation angle of the PIP joint can be obtained as follows:

$$\begin{aligned}\theta_2 &= \pi - \gamma_1 - \beta_2 \\ &= \pi - \arccos\left(\frac{(R+t_{1I})^2 + L_1^2 - (R+t_{0I})^2}{2(R+t_{1I})L_1}\right) \\ &\quad - \arccos\left(\frac{(R+t_{1I})^2 + L_2^2 - (R+t_{2I})^2}{2(R+t_{1I})L_2}\right) \\ &= f_2(L_1, L_2, t_{0I}, t_{1I}, t_{2I}; R)\end{aligned} \tag{6}$$

Finally, consider triangle $O_C J_{3I} T_I$, the angle β_3 is obtained as:

$$(R+t_{3I})^2 = (R+t_{2I})^2 + L_3^2 - 2(R+t_{2I})L_3\cos\beta_3$$

and

$$\beta_3 = \arccos\left(\frac{(R+t_{2I})^2 + L_3^2 - (R+t_{3I})^2}{2(R+t_{2I})L_3}\right) \tag{7}$$

From the geometry of the triangles and Eqns. (5) and (7) , the rotation angle at the DIP joint is obtained as follows:

$$\begin{aligned}\theta_3 &= \pi - \gamma_2 - \beta_3 \\ &= \pi - \arccos\left(\frac{(R+t_{2I})^2 + L_2^2 - (R+t_{1I})^2}{2(R+t_{2I})L_2}\right) \\ &\quad - \arccos\left(\frac{(R+t_{2I})^2 + L_3^2 - (R+t_{3I})^2}{2(R+t_{2I})L_3}\right) \\ &= f_3(L_2, L_3, t_{0I}, t_{1I}, t_{2I}, t_{3I}; R)\end{aligned} \tag{8}$$

As observed in Eqns. (3), (6) and (8), the joint rotation configuration can be determined by only a single parameter R given the fixed dimension of finger-thickness (i.e., t_{0I}, t_{1I}, t_{2I} and t_{3I}) and length of phalanges (L_1, L_2 and L_3). It is worth to note that the set of Eqns. (3), (6) and (8) represent a 1-DOF joint rotation configuration model of the human fingers. Furthermore, these angles are not coupled. The proposed model reduces the computational strain by utilizing a single variable which governs three angular values of each phalange, to harmoniously coordinate each finger for generating grasping motion based the profiles of R.

It is worth to note that the following constraints on R should be taken into consideration to obtain proper motion of a finger described in Eqs. (3), (6) and (8) from geometric viewpoint. The minimum R, $R_{\min}$ can be one greater than or equal to the largest value among Eqs. (9):

$$2R + t_{0I} - L_1 + t_{1I} > 0 \quad \rightarrow \quad R > \frac{L_1 - t_{0I} - t_{1I}}{2} \tag{9a}$$

$$2R + t_{1I} - L_2 + t_{2I} > 0 \quad \rightarrow \quad R > \frac{L_2 - t_{1I} - t_{2I}}{2} \tag{9b}$$

$$2R + t_{2I} - L_3 + t_{3I} > 0 \quad \rightarrow \quad R > \frac{L_3 - t_{2I} - t_{3I}}{2} \tag{9c}$$

The maximum radius $R_{\max}$ is chosen by assuming that the angle β_{0T} remains constant. Under this assumption, the value of R that satisfies the following equation is set to be R_{max}:

$$\sin\beta_{0T} = \frac{R}{R+t_{0I}},$$

By solving for R and letting R be R_{max} gives

$$R_{\max} = -\frac{t_{0I}\sin\beta_{0T}}{\sin\beta_{0T} - 1}.$$

3.2 Joint Configuration Model for the Thumb

With the notation in Fig. 5, a planar thumb model for joint rotation configuration can be derived in a similar manner. For triangle $O_C J_{1I} J_{1T}$, the angles β_{0T} and γ_{0T} are obtained as follows:

$$\begin{aligned}(R+t_{0T})^2 &= (R+t_{0I})^2 + L_{0T}^2 - 2(R+t_{0I})L_{0T}\cos\beta_{0T}\\ (R+t_{0I})^2 &= (R+t_{0T})^2 + L_{0T}^2 - 2(R+t_{0T})L_{0T}\cos\gamma_{0T}\end{aligned}$$

Solving equations above for β_{0T} and γ_{0T}, respectively, gives

$$\begin{aligned}\beta_{0T} &= \arccos\left(\frac{(R+t_{0I})^2 + L_{0T}^2 - (R+t_{0T})^2}{2(R+t_{0I})L_{0T}}\right)\\ &= \arccos\left(\frac{(t_{0I}-t_{0T})R + (t_{0I}^2 - t_{0T}^2 + L_{0T}^2)/2}{L_{0T}R + L_{0T}t_{0I}}\right) \qquad (10)\\ \gamma_{0T} &= \arccos\left(\frac{(R+t_{0T})^2 + L_{0T}^2 - (R+t_{0I})^2}{2(R+t_{0T})L_{0T}}\right)\\ &= \arccos\left(\frac{(t_{0T}-t_{0I})R + (t_{0T}^2 - t_{0I}^2 + L_{0T}^2)/2}{L_{0T}R + L_{0T}t_{0T}}\right) \qquad (11)\end{aligned}$$

The rotation angle at the MCP joint can be calculated by using Eqn. (10) as follows:

$$\begin{aligned}\theta_{0T} &= \frac{\pi}{2} + \beta_{0T}\\ &= \frac{\pi}{2} + \arccos\left(\frac{(t_{0I}-t_{0T})R + (t_{0I}^2 - t_{0T}^2 + L_{0T}^2)/2}{L_{0T}R + L_{0T}t_{0I}}\right)\\ &= -\pi + \underbrace{\arccos(0)}_{(=3\pi/2)} + \arccos\left(\frac{(t_{0I}-t_{0T})R + (t_{0I}^2 - t_{0T}^2 + L_{0T}^2)/2}{L_{0T}R + L_{0T}t_{0I}}\right)\\ &= f_0(L_{0T}, t_{0I}, t_{1T}; R) \qquad (12)\end{aligned}$$

For triangle $O_C J_{1T} J_{2T}$, the angles β_{1T} and γ_{1T} are obtained as follows:

$$\begin{aligned}(R+t_{1T})^2 &= (R+t_{0T})^2 + L_{1T}^2 - 2(R+t_{0T})L_{1T}\cos\beta_{1T}\\ (R+t_{0T})^2 &= (R+t_{1T})^2 + L_{1T}^2 - 2(R+t_{1T})L_{1T}\cos\gamma_{1T}\end{aligned}$$

Solving equations above for β_{1T} and γ_{1T}, respectively gives

$$\begin{aligned}\beta_{1T} &= \arccos\left(\frac{(R+t_{0T})^2 + L_{1T}^2 - (R+t_{1T})^2}{2(R+t_{0T})L_{1T}}\right)\\ &= \arccos\left(\frac{(L_{0T}-t_{1T})R + (t_{0T}^2 - t_{1T}^2 + L_{1T}^2)/2}{L_{1T}R + L_{1T}t_{0T}}\right) \qquad (13)\\ \gamma_{1T} &= \arccos\left(\frac{(R+t_{1T})^2 + L_{1T}^2 - (R+t_{0T})^2}{2(R+t_{1T})L_{1T}}\right)\\ &= \arccos\left(\frac{(t_{1T}-t_{0T})R + (t_{1T}^2 - t_{0T}^2 + L_{1T}^2)/2}{L_{1T}R + L_{1T}t_{1T}}\right) \qquad (14)\end{aligned}$$

By using Eqn. (10), (11) and (13), the rotation angle of the PIP joint can be obtained as follows:

$$\begin{aligned}\theta_{1T} &= -(\pi-\gamma_{0T}-\beta_{1T})\\ &= -\pi+\arccos\left(\frac{(t_{0T}-t_{0I})R+(t_{0T}^2-t_{0I}^2+L_{0T}^2)/2}{L_{0T}R+L_{0T}t_{0T}}\right)\\ &\quad+\arccos\left(\frac{(L_{0T}-t_{1T})R+(t_{0T}^2-t_{1T}^2+L_{1T}^2)/2}{L_{1T}R+L_{1T}t_{0T}}\right)\\ &= f_1(L_{0T},L_{1T},t_{0I},t_{0T},t_{1T};R)\end{aligned} \tag{15}$$

Finally, for triangle $O_C J_{2T} T_T$, the angle β_{3T} is obtained as:

$$(R+t_{3T})^2 = (R+t_{1T})^2+L_{3T}^2-2(R+t_{1T})L_{3T}\cos\beta_{3T}$$

and

$$\begin{aligned}\beta_{3T} &= \arccos\left(\frac{(R+t_{1T})^2+L_{3T}^2-(R+t_{3T})^2}{2(R+t_{1T})L_{3T}}\right)\\ &= \arccos\left(\frac{(t_{1T}-t_{3T})R+(t_{1T}^2-t_{3T}^2+L_{3T}^2)/2}{L_{3T}R+L_{3T}t_{1T}}\right)\end{aligned} \tag{16}$$

From the geometry of the triangles and Eqns. (14) and (16) , the rotation angle at the DIP joint is obtained as follows.

$$\begin{aligned}\theta_{3T} &= -(\pi-\gamma_{1T}-\beta_{3T})\\ &= -\pi+\arccos\left(\frac{(t_{1T}-t_{0T})R+(t_{1T}^2-t_{0T}^2+L_{1T}^2)/2}{L_{1T}R+L_{1T}t_{1T}}\right)\\ &\quad+\arccos\left(\frac{(t_{1T}-t_{3T})R+(t_{1T}^2-t_{3T}^2+L_{3T}^2)/2}{L_{3T}R+L_{3T}t_{1T}}\right)\\ &= f_3(L_{1T},L_{3T},t_{0T},t_{1T},t_{3T};R)\end{aligned} \tag{17}$$

Similarly, one should consider constraints on R for the proper motion of a thumb. For more details on extending the model to the rest of the fingers, as well as its experimental validation, refer to [28].

4 DESIGN AND ASSESSMENT OF THE ROBUST CLOSED LOOP ARTICULATED WEARABLE (CLAW) HAND FOR NATURAL MOTION

To illustrate the benefit of the proposed overall process, we perform optical motion capture of a subject performing precision grasping of a cylindrical pen using their thumb, index and middle fingertips (see Fig. 6). A challenging task of grasping a small object with high curvature is specifically chosen to explore the extent of the synthesis method to generalize to precision and power grasping of objects with different sizes and geometry. During each capture session, a subject sits such that their arm rests on the table in a relaxed position with a pen placed within their reach, and when prompted, grasps it with their fingertips.

Based on the trajectories of the markers, a planar serial 3*R* anthropometric backbone chain for each finger is synthesized, which best fits each consecutive limb's pose trajectory. After that, each 3*R* chain is constrained by a *PRR* chain, resulting in an eight-bar linkage. The design procedure for the middle, ring, and pinky fingers follow the procedure for the index finger closely and can be found in [25–27]. Details on the general design procedure for a four-bar mechanical thumb can be found in [32]. In what follows, the paper gives a brief overview of the synthesis process of the index finger and the thumb, followed by a detailed design candidate assessment for natural joint motion.

4.1 Synthesis and Assessment of an Index Finger Wearable Eight-bar Mechanism for Natural Motion

For the kinematic synthesis, two critical poses on the index finger trajectory are chosen with the finger fully extended and at the instance of grasp, where the local behavior is important for the finger motion. A velocity constraint is defined

Fig. 6. Optical motion capture of a subject performing grasping of a small pen using their thumb, index and middle fingers.

in the starting pose to control the finger's tangent motion upon flexion. A velocity and acceleration constraints compatible with fingertip-object contact and curvature constraints are defined in the second pose to mimic the grasping behavior in the vicinity of the contact. The velocity and acceleration constraints are computed from the optical motion capture data sampled at $100Hz$. The specific anthropometric limb/backbone chain dimensions for the index finger are $a_{34} = 38.9mm$ and $a_{45} = 18.3mm$, and $l_5 = 17.6mm$. For the PRR chain, we chose $a_{12} = 79.4mm$ with slide angle $\beta = 23^\circ$ (please refer to Fig. 3). Two RR chains $\mathbf{G}_1\mathbf{W}_1$ and $\mathbf{G}_2\mathbf{W}_2$ are computed to constrain the finger into an eight-bar linkage. Sixteen real solutions, able to follow the task fingertip trajectory, were obtained [25–27].

Linkage assessment criteria for testing the user-mechanism interference are used to sort the eight-bar design solutions. Specifically, the joint angles of the model were calculated via Eqn (3), (6), and (8) with the value of R corresponding to the coordinates of the fingertip Cartesian location under consideration. Next, the joint angles θ_i for the eight-bar backbone chain design candidates were compared to those obtained from the model (see Table 1 and Fig. 7). Finally, evaluation

Table 1. Comparison of joint angle configurations for index finger

Case		Fingertip			Joint angle		
		x_3 (mm)	y_3 (mm)	R (mm)	θ_1 (deg)	θ_2 (deg)	θ_3 (deg)
1	Desgin Candidate			–	20.25	18.36	19.25
	Model	48.75	46.57	38	23.46	26.24	18.09
2	Desgin Candidate			–	21.35	18.80	19.84
	Model	50.93	13.45	33	25.25	29.15	20.18
3	Desgin Candidate			–	37.54	21.11	31.94
	Model	54.72	-24.50	22	31.14	38.91	27.21

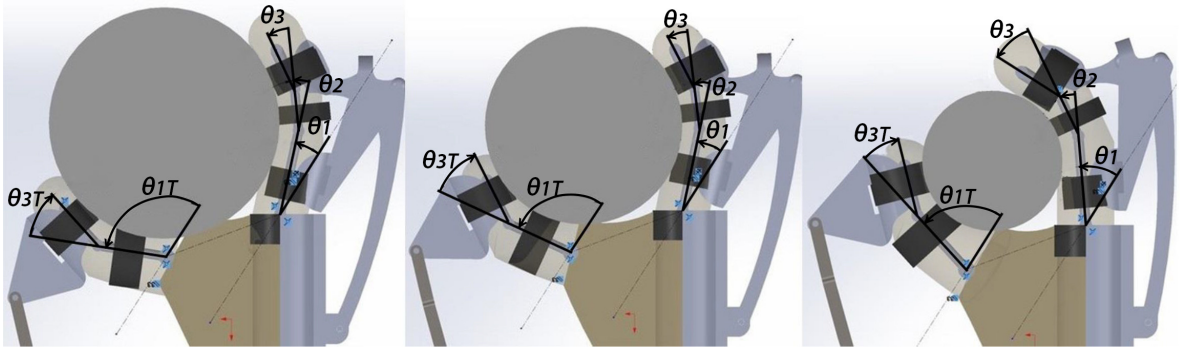

Fig. 7. Backbone chain joint angle results for the chosen index finger and thumb design candidates.

of the natural joint motion coordination ability of the backbone chain of the sorted solution(s) is tested. Figure 8 shows the chosen index finger design going through the specified task consisting of initial and final positions, two velocities and one acceleration (in Mathematica).

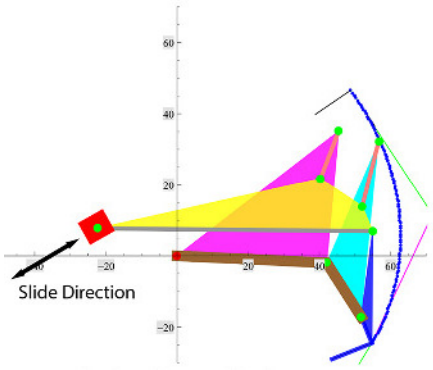

Fig. 8. The index finger, moving through the specified physiological task with first and second order task constraints.

The assessment results in Table 1 show an average difference of about 3.3° between the joint angles obtained from the "naturalistic" model described in the previous section and those of the synthesized index finger. This is expected, due to the constrained nature of the eight-bar linkage, possibly leading to the wearer making conscious modifications/compensations to the movement. The CAD drawing of the selected eight-bar index finger can be seen in Fig. 9.

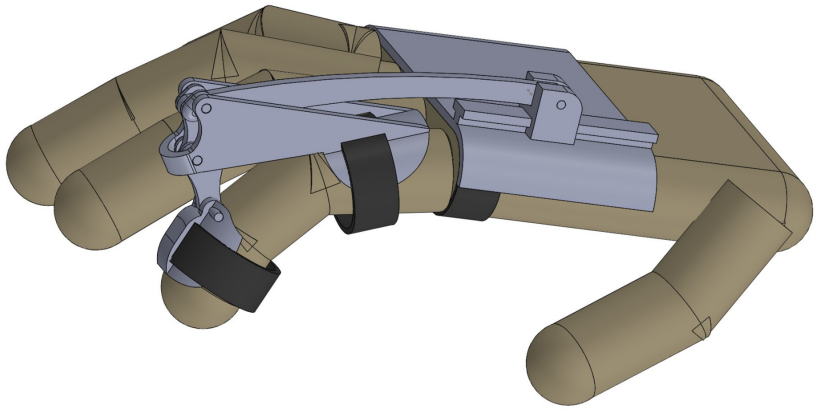

Fig. 9. CAD drawing of the selected eight-bar index finger with the backbone chain replaced by the human limb, thus providing the skeletal structure of the resulting wearable device.

4.2 Assessment of a Four-bar Wearable Thumb Mechanism for Natural Motion

The wearable thumb was designed as a planar parallel *RRRP* four-bar slider with an anthropometric *RR* backbone chain. Like the index finger design, the kinematic task was obtained using an optical motion capture system and consisted of initial and final positions with two velocities and one acceleration. The subject's anthropometric size of the thumb was $l_1 = 37mm$ and $l_2 = 32mm$. The synthesis resulted in two possible design candidates. More details on the design of four-bar linkages with contact and curvature task constraints can be found in [32].

After testing for user-device interference, the ability of the chosen four-bar mechanical thumb for the natural movement was assessed. The joint angles of the model were calculated with the value of R corresponding to the coordinates of the fingertip cartesian location under consideration. Next, the joint angles θ_i for each four-bar finger's backbone chain design candidate were compared to those obtained from the model (see Table 2 and Fig. 7). Figure 10 represents the chosen mechanical thumb design, moving through the specified task with higher-order constraints (in Mathematica).

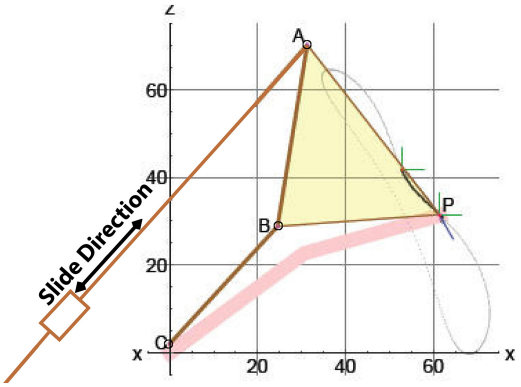

Fig. 10. The mechanical thumb, moving through the specified physiological task with first and second order task constraints.

Table 2. Comparison of joint angle configurations for thumb

Case		Thumb tip			Joint angle	
		x_3 (mm)	y_3 (mm)	R (mm)	θ_{1_T} (deg)	θ_{3_T} (deg)
1	Design Candidate			–	113.98	-39.41
	Model	52.78	41.78	38	105.40	-51.01
2	Design Candidate			–	98.03	-38.92
	Model	55.81	38.55	33	99.15	-48.16
3	Design Candidate			–	75.09	-27.81
	Model	61.42	31.33	22	78.57	-38.45

On average, the assessment results show about 4.8° difference between the joint angles obtained from the "naturalistic" model, described in the previous section, and those of the synthesized thumb. Similar to the index finger, this is expected due to the constrained nature of the four-bar linkage, possibly leading to the wearer making conscious modifications/compensations to the movement.

The CAD drawing of the assembled CLAW hand is shown in Fig. 11. Although the CLAW hand design can actuate each finger independently, it is currently set up for users to operate their impaired hand by either moving one of their finger joints or driving it passively with their healthy arm. This is achieved by coupling all the fingers and thumb linkage to yield one degree of freedom mechanism using a common slider.

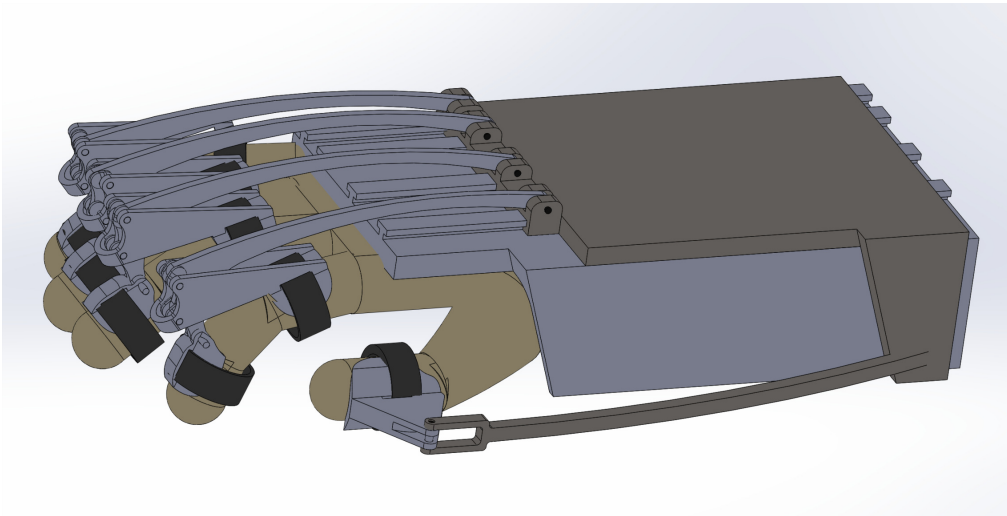

Fig. 11. The resulting one degree of freedom 3D printed prototype of the passive CLAW hand performing a grasping task. The user can operate the arm by either moving one their finger(s), or by using their healthy arm through a common slider.

5 Preliminary Testing of CLAW Hand

Preliminary experimental testing with healthy subjects wearing the prototype (Fig. 11) developed in Section 4 was performed. The goal is to incorporate the various lessons learned from this preliminary study to develop a final prototype and pave the way for more design studies in the future.

5.1 CLAW Hand Design Wearability

Wearability of the device was assessed mainly through a set of developed criteria, shown in Table 3. For each measure,

Table 3. Level of Effect

	Metric and Units		Level of Effect				
Effect	*Metric*	*Units*	*Low*	*Moderate*	*Large*	*VeryLarge*	*Extreme*
Energy Cost	Heart Rate	beats per minute	up to 90	91-110	111-130	131-150	>151
	Relative Perceived Exertion	Borg RPE score	6-9	10-11	12-13	14-15	16-20
Comfort	General Wearable	CRS score	0-4	5-8	9-12	13-16	17-20
	Musculoskeletal Loading	Borg CR-10 score	0-4	5-8	9-12	13-16	17-20

the value obtained from an assessment can be associated to a level of effect ranging from 'Low' to 'Extreme'. These levels can be determined from values published for heart rate data [33], descriptors used on the Borg RPE and CR-10 scales [34], and action levels published with the REBA method [35]. For the comfort scales the levels of effect were determined by proportioning the scales into equal parts. From the levels of effect, the following five Wearability Levels (WL) can be suggested: (i) Low: Device is wearable; (ii) Moderate: Device is wearable, but changes may be necessary; (iii) Large: Device is wearable, but changes are advised, uncomfortable; (iv) Very Large: Device is not wearable, fatiguing and very uncomfortable; (v) Extreme: Device is not wearable, extremely stressful and potentially harmful.

Specifically, the wearability assessment involved an evaluation of the physiological (Relative Perceived Exertion RPE score) and comfort (Comfort Rating CR score) effects. The selected method for physiological assessment was related to the level of energy spent to operate the device while performing a specific grasping task. The comfort category assessment referred to localized discomfort due to musculoskeletal loading in the sense of (i) attachment, (ii) harm, and (iii) movement. The attachment was related to the level of the physical sensation of the device on the wearer's hand; harm incorporated physical sensation conveying pain, and movement was related to the wearer making conscious modifications/compensations to the movement.

5.1.1 Methods

A total of five healthy male participants, ages 20 - 35, took part in the preliminary testing. The subjects were specifically chosen to have hand anthropometric data similar to the test subject for which the CLAW hand was designed. As an example, the specific anthropometric limb/backbone chain dimensions for the index fingers were in the range of $a_{34} = 38 - 40mm$ and $a_{45} = 18 - 20mm$, and $l_5 = 17 - 20mm$. The dimensions for the thumb were in the range between $l_1 = 36 - 38mm$ and $l_2 = 30 - 33mm$. The device's performance was generally assessed through testing the ability of the user wearing the CLAW hand to perform both precision and power grasping of a variety of symmetrical objects (see Fig. 12). After putting on the CLAW hand, each participant gave a pre-test value for their perceived exertion using the Borg RPE scale. After interacting with the CLAW hand, each participant gave a post-test value for their perceived exertion, pointed out any areas of pain and discomfort, and rated the pain using the Borg CR-10 scale.

5.1.2 Results

The wearability assessment results for energy cost and comfort effects are shown in Table 4. The user trials lasted on average between 4-5 minutes. The majority of male participants rated Energy cost in the Low level, suggesting that the CLAW hand device does not exert a large physiological demand (see Table 4). However, the post-test rating was higher than the pre-test, indicating that the device may be fatigued if worn for prolonged periods.

The majority of scores for each comfort dimension were in the Low to Moderate levels (see Table 4). The ratings related to Attachment and Movement highlight that the wearers were conscious of wearing the device and were making some minor conscious modifications/compensations to its movement. This will be further addressed in the future.

In general, the preliminary experimental testing showed that the 3D printed prototype of the CLAW hand could successfully guide the user's fingers without causing discomfort, ensuring both precision and power grasping of a wide range of symmetrical objects with different sizes in a natural manner.

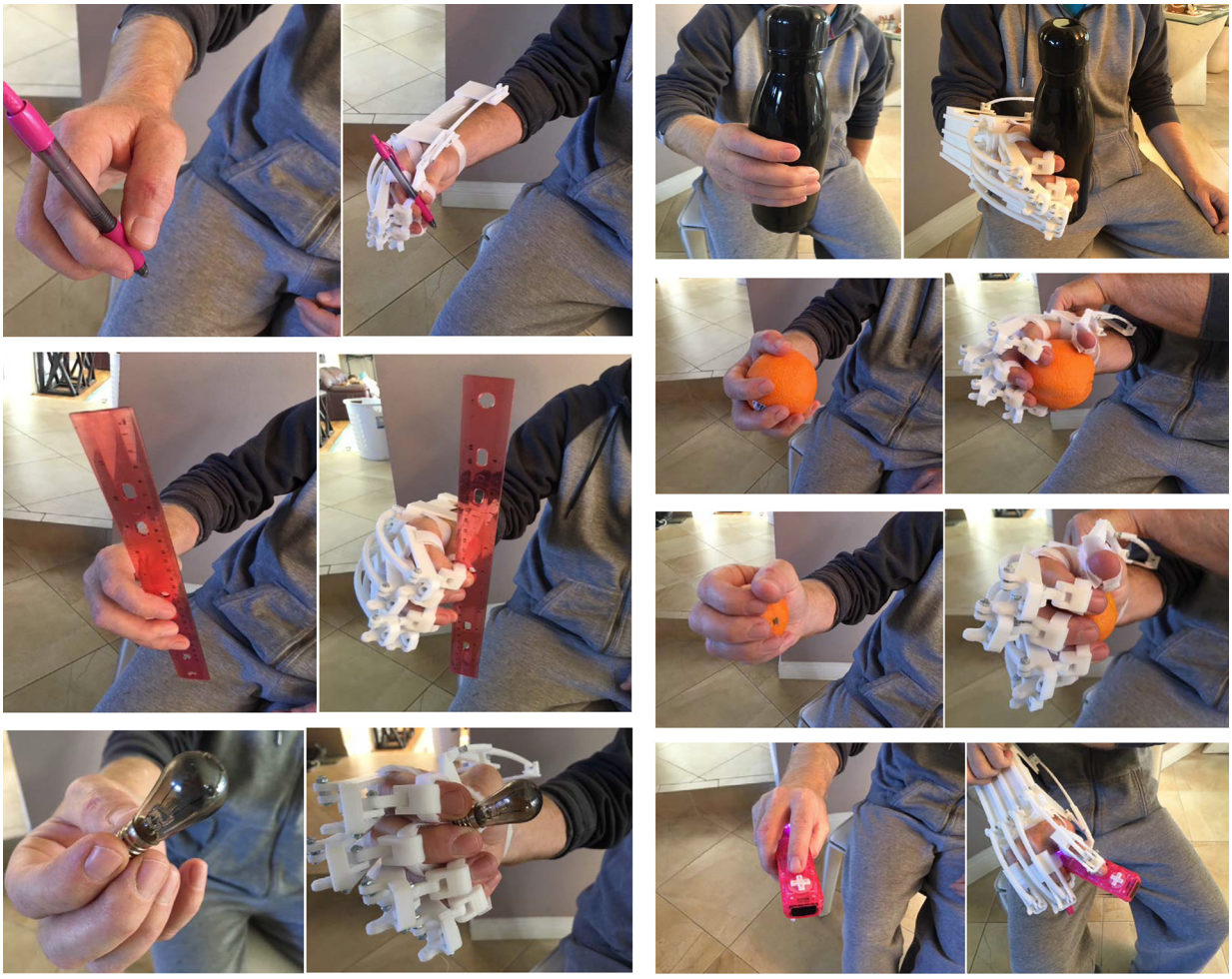

Fig. 12. CLAW hand precision (left) and power (right) grasp performance experimental testing with male subjects.

Table 4. Wearability Ratings Results: Value Represents the Number of Participants (N=5) Rating Each Variable within the 5 Levels of Effect

Effect		Level of Effect				
		Low	*Moderate*	*Large*	*VeryLarge*	*Extreme*
Energy Cost (Relative Perceived Exertion RPE Score)	Pre-Test	4	1	0	0	0
	Post-Test	3	2	0	0	0
Comfort (Comfort Rating CR Score)	Attachment	3	1	1	0	0
	Harm	5	0	0	0	0
	Movement	4	1	0	0	0

5.2 CLAW Hand Design Scalability

Pilot testing on the generalization of the CLAW hand design to other hand sizes was evaluated through four healthy female subjects, two of which were between 15 and 18 years of age and the other two between 45 and 75 years of age. The subjects were specifically chosen to have a wider range of hand/finger anthropometric data than the five male test subjects. For example, the specific anthropometric limb/backbone chain dimensions for the index fingers were in the range of $a_{34} = 25 - 35mm$ and $a_{45} = 15 - 25mm$, and $l_5 = 15 - 25mm$. The dimensions for the thumb were ranging between $l_1 = 25 - 35mm$ and $l_2 = 20 - 30mm$. Similar to the first experiment, the device's performance was generally assessed through testing the ability of the user wearing the CLAW hand to perform both precision and power grasping of a variety of symmetrical objects, used in the first trial (see Fig. 13). The user trials lasted on average between 4-5 minutes.

After putting on the CLAW hand, each female participant gave a pre-test value for their perceived exertion using the Borg RPE scale. Similarly, after interacting with the CLAW hand, each participant gave a post-test value for their perceived exertion, pointed out any areas of pain and discomfort, and rated the pain using the Borg CR-10 scale. The wearability assessment results for energy cost and comfort effects are shown in Table 5. Similarly to the first experiment, the majority of participants rated Energy cost in the Low level, suggesting that the CLAW hand device does not exert a large physiological

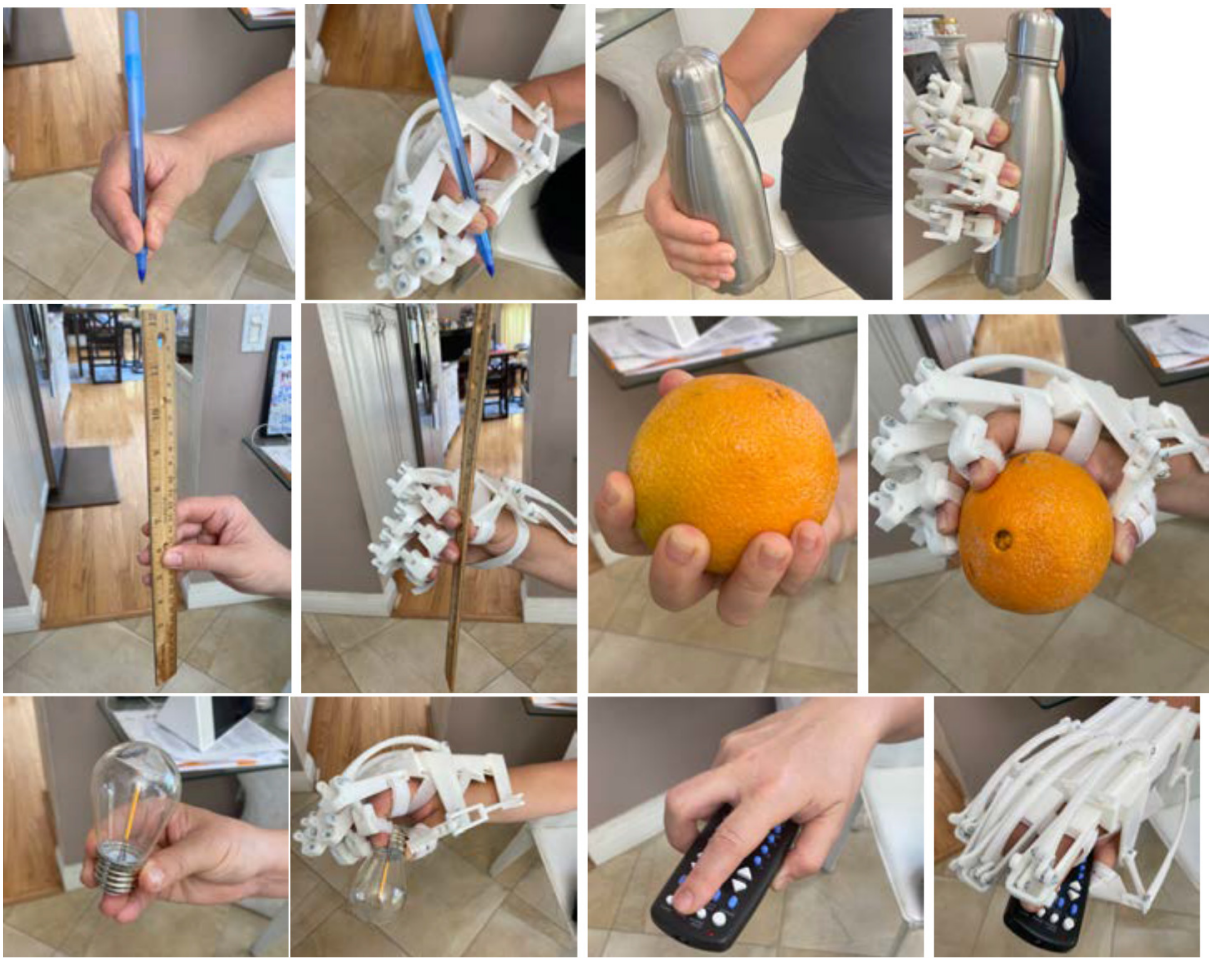

Fig. 13. CLAW hand precision (left) and power (right) grasp performance experimental testing with female subjects.

demand (see Table 5). The post-test rating indicated that the device was not causing fatigue when worn for prolonged periods. The majority of scores for each comfort dimension were in the Low level (see Table 5). The ratings related to Attachment, Harm, and Movement highlight that the wearers were conscious of wearing the device and were not making conscious modifications/compensations to its movement.

Table 5. Wearability Ratings Results: Value Represents the Number of Participants (N=4) Rating Each Variable within the 5 Levels of Effect

Effect		Level of Effect				
		Low	*Moderate*	*Large*	*VeryLarge*	*Extreme*
Energy Cost (Borg Relative Perceived Exertion Score)	Pre-Test	4	0	0	0	0
	Post-Test	3	1	0	0	0
Comfort (Comfort Rating Score)	Attachment	3	1	0	0	0
	Harm	4	0	0	0	0
	Movement	4	0	0	0	0

In general, the preliminary scalability experimental testing showed that the 3D printed prototype of the CLAW hand could successfully guide the user's fingers without causing discomfort while ensuring both precision and power grasping of a wide range of symmetrical objects with different sizes in a natural manner. Also, it should be noted that the comfort rating scores from the scalability test related to the smaller female hands were slightly better than those from the male tests. This implies the ability of the CLAW hand to generalize to different hand/finger sizes and will be investigated further.

6 CONCLUSIONS

This work presents an assessment procedure and testing on the wearability of our one degree of freedom multi-loop wearable mechanical hand that is passively driven by a slider. The results show that it can be successfully utilized for adaptive and precision grasping of different size objects. The paper gives a brief overview of how to design such devices. It includes capturing and deriving the physiological task requirements, compatible with finger-object contact and curvature constraints, anthropometric backbone chain specification, and dimensional synthesis. Once it is ensured that the synthesized mechanism tip motion is close to the physiological precision grasping tip trajectories, linkage performance assessment criteria related to user-device interference and joint angle natural motion, based on recently developed geometric joint coordination models, are proposed. At the end of the design process, the wearer's limb replaces the mechanism backbone chain to provide the skeletal structure for the customized passive wearable hand device.

Preliminary test results with a limited set of male and female healthy subjects show that the CLAW hand can generalize to several different finger and hand dimensions. It is easy to operate and guides the user's fingers without causing high-level discomfort, and ensures physiological precision and power grasping naturally. Unlike other wearable device design techniques that use parallel mechanical linkages on the limbs, here we offer a novel geometric design process to create robust wearable four and eight-bar linkages that incorporate initial anthropometric backbone chain and physiological task for natural motion using a minimal number of actuators (or no actuators). All aspects of the geometric design process are explained, from physiological task acquisition, to anthropometric backbone chain specification, to dimensional synthesis, to user-design candidate interference evaluation, and assessment of the design candidates. The resulting CLAW hand incorporates sliding joints, one at each finger, that allow for fitting to different human finger sizes (within a specific range) and grasping a variety of symmetrical objects with different shapes and geometries. The lack of electrical actuators and sensors simplifies the control, resulting in a lightweight and cost-effective solution. Currently, the motion of all fingers is coupled, which presents a challenge for certain tasks that require independent finger motion. Future research includes considering actuation strategies to enable active finger motion independently.

7 ACKNOWLEDGMENTS

The authors gratefully acknowledge the support of the National Science Foundation (NSF), award Id #1751770, the 2018 Research-Year Grant of Jeonju University, and SUTD Growth Plan Grant No. SGPHCRS1905.

References

[1] Dollar, A. M., and Herr, H., 2008. "Lower extremity exoskeletons and active orthoses: challenges and state-of-the-art". *IEEE Transactions on robotics,* ***24***(1), pp. 144–158.

[2] Yang, C., Zhang, J., Chen, Y., Dong, Y., and Zhang, Y., 2008. "A review of exoskeleton-type systems and their key technologies". *Proceedings of the Institution of Mechanical Engineers, Part C: Journal of Mechanical Engineering Science,* ***222***(8), pp. 1599–1612.

[3] Bogue, R., 2009. "Exoskeletons and robotic prosthetics: a review of recent developments". *Industrial Robot: an international journal,* ***36***(5), pp. 421–427.

[4] Gopura, R., and Kiguchi, K., 2009. "Mechanical designs of active upper-limb exoskeleton robots: State-of-the-art and design difficulties". In 2009 IEEE International Conference on Rehabilitation Robotics, IEEE, pp. 178–187.

[5] Gopura, R., Kiguchi, K., and Bandara, D., 2011. "A brief review on upper extremity robotic exoskeleton systems". In 2011 6th international Conference on Industrial and Information Systems, IEEE, pp. 346–351.

[6] Heo, P., Gu, G. M., Lee, S.-j., Rhee, K., and Kim, J., 2012. "Current hand exoskeleton technologies for rehabilitation and assistive engineering". *International Journal of Precision Engineering and Manufacturing,* ***13***(5), pp. 807–824.

[7] Worsnopp, T., Peshkin, M., Colgate, J., and Kamper, D., 2007. "An actuated finger exoskeleton for hand rehabilitation following stroke". In 2007 IEEE 10th international conference on rehabilitation robotics, IEEE, pp. 896–901.

[8] Nakagawara, S., Kajimoto, H., Kawakami, N., Tachi, S., and Kawabuchi, I., 2005. "An encounter-type multi-fingered master hand using circuitous joints". In Proceedings of the 2005 IEEE International Conference on Robotics and Automation, IEEE, pp. 2667–2672.

[9] Fontana, M., Dettori, A., Salsedo, F., and Bergamasco, M., 2009. "Mechanical design of a novel hand exoskeleton for accurate force displaying". In 2009 IEEE International Conference on Robotics and Automation, IEEE, pp. 1704–1709.

[10] Chiri, A., Vitiello, N., Giovacchini, F., Roccella, S., Vecchi, F., and Carrozza, M. C., 2011. "Mechatronic design and characterization of the index finger module of a hand exoskeleton for post-stroke rehabilitation". *IEEE/ASME Transactions on mechatronics,* ***17***(5), pp. 884–894.

[11] Yeow, C.-H., Baisch, A., Talbot, S., and Walsh, C., 2014. "Cable-driven finger exercise device with extension return springs for recreating standard therapy exercises". *Journal of Medical Devices,* ***8***(1), p. 014502.

[12] Ma, Z., and Ben-Tzvi, P., 2015. "Design and optimization of a five-finger haptic glove mechanism". *Journal of Mechanisms and Robotics,* ***7***(4), p. 041008.

[13] Birglen, L., and Gosselin, C. M., 2005. "Geometric design of three-phalanx underactuated fingers". *Journal of Mechanical Design,* ***128***(2), pp. 356–364.
[14] Wege, A., and Hommel, G., 2005. "Development and control of a hand exoskeleton for rehabilitation of hand injuries". In 2005 IEEE/RSJ International Conference on Intelligent Robots and Systems, IEEE, pp. 3046–3051.
[15] Wang, J., Li, J., Zhang, Y., and Wang, S., 2009. "Design of an exoskeleton for index finger rehabilitation". In 2009 Annual International Conference of the IEEE Engineering in Medicine and Biology Society, IEEE, pp. 5957–5960.
[16] Fontana, M., Fabio, S., Marcheschi, S., and Bergamasco, M., 2013. "Haptic hand exoskeleton for precision grasp simulation". *Journal of Mechanisms and Robotics,* ***5***(4), p. 041014.
[17] Gosselin, C. M., and Laliberte, T., 1998. Underactuated mechanical finger with return actuation, June 9. US Patent 5,762,390.
[18] Baek, S.-F., Lee, S.-H., and Chang, J. H., 1999. "Design and control of a robotic finger for prosthetic hands". In Proceedings 1999 IEEE/RSJ International Conference on Intelligent Robots and Systems. Human and Environment Friendly Robots with High Intelligence and Emotional Quotients (Cat. No. 99CH36289), Vol. 1, IEEE, pp. 113–117.
[19] Fukaya, N., Toyama, S., Asfour, T., and Dillmann, R., 2000. "Design of the tuat/karlsruhe humanoid hand". In Proceedings. 2000 IEEE/RSJ International Conference on Intelligent Robots and Systems (IROS 2000)(Cat. No. 00CH37113), Vol. 3, IEEE, pp. 1754–1759.
[20] Sergi, F., Accoto, D., Tagliamonte, N. L., Carpino, G., and Guglielmelli, E., 2011. "A systematic graph-based method for the kinematic synthesis of non-anthropomorphic wearable robots for the lower limbs". *Frontiers of Mechanical Engineering,* ***6***(1), pp. 61–70.
[21] Accoto, D., Sergi, F., Tagliamonte, N. L., Carpino, G., Sudano, A., and Guglielmelli, E., 2014. "Robomorphism: a nonanthropomorphic wearable robot". *IEEE Robotics & Automation Magazine,* ***21***(4), pp. 45–55.
[22] Agarwal, P., Hechanova, A., and Deshpande, A. D., 2013. "Kinematics and dynamics of a biologically inspired index finger exoskeleton". In Dynamic Systems and Control Conference, Vol. 56130, American Society of Mechanical Engineers, p. V002T28A001.
[23] Soh, G. S., and Robson, N., 2013. "Kinematic synthesis of minimally actuated multi-loop planar linkages with second order motion constraints for object grasping". In Dynamic Systems and Control Conference, Vol. 56147, American Society of Mechanical Engineers, p. V003T38A004.
[24] Robson, N., and Soh, G. S., 2014. "Geometric design of minimally actuated exoskeletons". In Proc. of 36th Annual International Conference of the IEEE Engineering in Medicine and Biology Society,(EMBC/14), Chicago, IL.
[25] Robson, N., and Soh, G. S., 2016. "Geometric design of eight-bar wearable devices based on limb physiological contact task". *Mechanism and Machine Theory,* ***100***, pp. 358–367.
[26] Tan, G. R., Robson, N., and Soh, G. S., 2016. "Dimensional synthesis of a passive eight-bar slider exo-limb for grasping tasks". In International Design Engineering Technical Conferences and Computers and Information in Engineering Conference, Vol. 50169, American Society of Mechanical Engineers, p. V05BT07A039.
[27] Tan, G. R., Robson, N., and Soh, G. S., 2017. "Motion generation of passive slider multiloop wearable hand devices". *Journal of Mechanisms and Robotics,* ***9***(4), p. 041011.
[28] Won, J.-S., and Robson, N., 2019. "Control-oriented finger kinematic model: geometry-based approach". *Journal of Mechanisms and Robotics,* ***11***(6), p. 061007.
[29] Robson, N., and McCarthy, J. M., 2007. "Kinematic synthesis with contact direction and curvature constraints on the workpiece". In International Design Engineering Technical Conferences and Computers and Information in Engineering Conference, Vol. 48094, pp. 581–588.
[30] Soh, G. S., and Ying, F., 2013. "Dimensional synthesis of planar eight-bar linkages based on a parallel robot with a prismatic base joint". In International Design Engineering Technical Conferences and Computers and Information in Engineering Conference, Vol. 55935, American Society of Mechanical Engineers, p. V06AT07A051.
[31] Soh, G. S., and Ying, F., 2015. "Motion generation of planar six-and eight-bar slider mechanisms as constrained robotic systems". *Journal of Mechanisms and Robotics,* ***7***(3), p. 031018.
[32] Ghosh, S., and Robson, N., 2014. "Development of a one degree of freedom mechanical thumb based on anthropomorphic tasks for grasping applications". In *Advances in Robot Kinematics*. Springer, pp. 335–344.
[33] Åstrand, P.-O., Rodahl, K., Dahl, H. A., and Strømme, S. B., 2003. *Textbook of work physiology: physiological bases of exercise*. Human kinetics.
[34] Borg, G., 1975. "Simple rating for estimation of perceived exertion". *Physical work and effort*, pp. 39–46.
[35] McAtamney, L., and Hignett, S., 1995. "Reba: a rapid entire body assessment method for investigating work related musculoskeletal disorders". In Proceedings of the 31st annual conference of the Ergonomics Society of Australia, Melbourne: The Society, pp. 13–15.

List of Figures

List of Tables